International Journal of Nanomedicine

Dovepress
open access to scientific and medical research

Open Access Full Text Article

ORIGINAL RESEARCH

Ethosome-Derived Invasomes as a Potential Transdermal Delivery System for Vardenafil Hydrochloride: Development, Optimization and Application of Physiologically Based Pharmacokinetic Modeling in Adults and Geriatrics

This article was published in the following Dove Press journal:
International Journal of Nanomedicine

Hussein O Ammar[1]
Mina Ibrahim Tadros[2]
Nahla M Salama[1]
Amira Mohsen Ghoneim[1]

[1]Department of Pharmaceutics and Pharmaceutical Technology, Faculty of Pharmaceutical Sciences and Pharmaceutical Industries, Future University in Egypt (FUE), New Cairo, Egypt; [2]Department of Pharmaceutics and Industrial Pharmacy, Faculty of Pharmacy, Cairo University, Cairo, Egypt

Aim: The aim of the current work was to develop vardenafil hydrochloride (VRD)-loaded ethosome-derived invasomes as a possible transdermal system which could be used for patients suffering from pulmonary arterial hypertension.

Methods: VRD-loaded ethosomes were developed at three concentrations of phosphatidylcholine (5, 10 and 15 mg/mL) and three percentages of ethanol (20%, 30% and 40%, v/v). The best achieved VRD-loaded ethosomes (ETH9) were optimized to invasomes via incorporation of terpenes (limonene, cineole and a 1:1 mixture) at three concentrations (0.5%, 1% and 2%, v/v). All systems were evaluated for vesicle size, zeta potential, drug entrapment efficiency (EE%), cumulative drug permeated percentages after 0.5hrs ($Q_{0.5h}$) and 12hrs (Q_{12h}) and steady-state flux (J_{ss}). The optimized system (ETH9-INV8) was further characterized for morphology, histopathology and confocal laser scanning microscopy (CLSM). Physiologically based pharmacokinetic (PBPK) modeling was employed to estimate VRD pharmacokinetic parameters from the optimized transdermal system and an oral aqueous drug dispersion, in adults and geriatrics.

Results: The optimized invasomal system (ETH9-INV8) was characterized with spherical vesicles (159.9 nm) possessing negative zeta potential (−20.3 mV), promising EE% (81.3%), low $Q_{0.5h}$ (25.4%), high Q_{12h} (85.3%) and the largest steady-state flux (6.4 $\mu g.cm^{-2}h^{-1}$). Following a leave-on period of 12hrs in rats, it showed minor histopathologic changes. CLSM studies proved its ability to deeply permeate rat skin. Lower C_{max} values, delayed T_{max} estimates and greater $AUC_{0\text{-}24h}$ folds in adults and geriatrics (≈ 2.18 and 1.69, respectively) were estimated following the transdermal application of ETH9-INV8 system.

Conclusion: ETH9-INV8 is a promising transdermal system for VRD.

Keywords: vardenafil hydrochloride, ethosomes, invasomes, transdermal, physiologically based pharmacokinetic modeling

Correspondence: Mina Ibrahim Tadros
Department of Pharmaceutics and Industrial Pharmacy, Faculty of Pharmacy, Cairo University, Cairo 11562, Egypt,
Tel +20 1223620458
Fax +20 223628246
Email mina.tadros@pharma.cu.edu.eg

Introduction

Pulmonary arterial hypertension (PAH) is a radical syndrome identified by a raise of pulmonary artery pressure and pulmonary vascular resistance, eventually causing right ventricular failure and mortality.[1] The pathogenesis of this disease is poorly inferred. However, the manner of development of PAH has been investigated,

including, inflammation, an imbalance between vascular cell proliferation and apoptosis and extreme vasoconstriction. All these stages result in narrowing of the pulmonary arteriolar lumens and increasing pulmonary vascular resistance.[2,3] Patients suffering from PAH endure breathlessness, inability to function and poor quality of life. Among the risk factors of PAH are old age, hypertension, diabetes and coronary artery disease.[4]

PAH is accompanied with defective release of nitric oxide,[5] caused by reduced expression of nitric oxide synthase in the vascular endothelium of pulmonary arteries.[6] Recently, phosphodiesterase-5 (PDE-5) inhibitors exhibited some potential in the management of PAH. PDE-5 is an isoenzyme that metabolizes cyclic guanosine monophosphate resulting in blood vessel constriction.[7] Interestingly, PDE-5 is plentifully expressed in lung tissue and hence, could be considered as a promising target for PAH treatment.[8] PDE-5 inhibitors, like sildenafil, enhance the levels of cyclic guanosine monophosphate, which could maintain the antiproliferative[9] and vasodilating[10] effects of endogenous nitric oxide. Sildenafil[11] and tadalafil[12] have demonstrated efficacy in patients suffering from PAH. Vardenafil (VRD) is more potent than sildenafil or tadalafil in inhibiting PDE-5.[13,14] In a study by Karasu-Minareci et al,[8] the efficiency of VRD in the treatment of PAH-induced rats was elucidated. According to the randomized, double-blind, placebo-controlled study of Jing et al,[15] it was proved that VRD was effective and well tolerated in patients with PAH at a dose of 5 mg. VRD is formulated as immediate-release film-coated tablets, at 2.5–20 mg doses. Unfortunately, the therapeutic efficiency of the drug following oral administration is hampered by certain limitations, including, low aqueous solubility (0.11 mg/mL), short biological half-life (≈ 4–5hrs) and limited oral bioavailability (15%) due to pre-systemic and hepatic first-pass metabolism.[16] In an attempt to surmount such limitations and offer a non-invasive medication, ethosomes were developed for the transdermal delivery of VRD for the treatment of erectile dysfunction.[17] Herein, VRD-loaded ethosome-derived invasomal systems were designed and optimized as a promising transdermal drug delivery system which could be used for the management of PAH. Ethosomes are vesicular systems containing phospholipids and ethanol. Compared to conventional liposomes, these soft vesicles exhibit improved transdermal permeation capabilities. Ethanol is a well-known permeation enhancer. It acts by disturbing the ordered multilamellar lipid domain, decreasing its structure density, enhancing the fluidity of stratum corneum (SC) and thus providing the vesicles with enough flexibility to deeply permeate the skin layers.[18] Recently, invasomes were introduced as vesicular systems containing phospholipids, ethanol as well as a single or a mixture of terpenes. Compared to ethosomes, the incorporation of terpenes adds extra advantages with respect to breaking the hydrogen bonds in SC, disrupting their tight bilayers and lipid packing and promoting drug permeation through the intercellular lipids.[19]

The application of physiologically based pharmacokinetic (PBPK) modeling had attracted great attention in the last years as a novel approach to estimate the drug pharmacokinetics following administration in one or more populations via a modeling software.[20] PBPK modeling enables the prediction of drug plasma concentration–time curves based on the results of the in vitro and ex vivo characterization studies as well as the physicochemical properties of the drug. Prior verification of the model with the published clinical pharmacokinetic data is needed.[21] PBPK modeling is currently investigated in pharmaceutical research and development and in health risk assessment as a valuable resource for decision-making at various drug development stages.[21,22]

In the current work, the multi-phase multi-layer mechanistic dermal absorption (MPML-MechDermA) model was investigated for the estimation of VRD pharmacokinetic parameters following the transdermal application of the optimized ethosome-derived invasomal system in adults and in geriatrics using Simcyp® Simulator V17.1 software (Certara, Sheffield, UK). According to this model, a brick and mortar structure was proposed to represent the SC. The corneocytes (the cuboid bricks) are immersed in the lipid matrix (the mortar). This structure illustrates the tight-packing mosaic arrangement of corneocytes with intercellular lipids. It could be used to simulate the complex pathway for drug diffusion via the SC.[23]

Materials and Methods

Materials

Vardenafil hydrochloride (VRD) was kindly donated by Marcyrl Pharmaceutical Industries (Cairo, Egypt). L-α-phosphatidylcholine (PC, Type IV-S), acetonitrile (HPLC grade), ethanol (HPLC grade) and Rhodamine B were purchased from Sigma-Aldrich Chemical Co. (St. Louis, MO). D-Limonene and 1.8-cineole were derived from Thermo Fisher Scientific GmbH (Karlsruhe, Germany). Sodium chloride, potassium chloride, di-sodium hydrogen phosphate and sodium di-hydrogen phosphate were supplied from El-Nasr Pharmaceutical Chemicals Co. (Cairo, Egypt).

Preparation of VRD-Loaded Ethosomes (ETHs)

The ethanol injection technique was adopted for the development of VRD-loaded ethosomes, at 25 ± 0.5 ºC, with slight modifications.[24] Briefly, PC and VRD were dissolved in ethanol. The alcoholic solution was injected into distilled water at a flow rate of 1 mL/min with magnetic stirring (1500 rpm).

The ethosomes were formed spontaneously and turned the resulting hydroalcoholic solution slightly turbid. The developed ethosomes were finely homogenized (5000 rpm) (Heidolph Silent Crusher M, Schwabach, Germany) for 3 cycles (1.5 min, each) with 5 min rest in-between. The final concentration of VRD was 5 mg/mL. The composition of the investigated VRD-loaded ETHs is shown in Table 1.

Preparation of VRD-Loaded Invasomes (INVs)

For optimization of the best achieved VRD-loaded ETH, VRD-loaded invasomes (INVs) were developed following the incorporation of terpenes (cineole, limonene or a 1:1 mixture of limonene and cineole) into the alcoholic solution of PC and VRD. The final concentration of VRD was 5 mg/mL. The composition of the investigated VRD-loaded INVs is shown in Table 2.

Design of Experiments

For the developed VRD-loaded ETHs, the response surface design was utilized to study the influence of two independent variables at three levels, viz., (i) PC concentration (5, 15 and 25 mg/mL) and (ii) ethanol percentage (20%, 30% and 40% v/v). Thirteen sets of experimental runs were constructed, via the central composite design, for nine investigated systems using Minitab Statistical Software (Minitab® 17, State College, PA). The central point was repeated to minimize the experimental error.

For the optimized VRD-loaded ETH-derived INVs, the multilevel factorial design was adopted to investigate the effect of two independent variables at three levels, viz., (i) terpene type (limonene, cineole and a 1:1 mixture of limonene and cineole) and (ii) terpene concentration (0.5%, 1% and 2% v/v).

In all systems, five responses were evaluated, viz., vesicle size, drug entrapment efficiency percentage (EE%), cumulative drug permeated percentages after 0.5 h ($Q_{0.5h}$) and 12 h (Q_{12h}) and the steady-state flux (J_{ss}).

Characterization of VRD-Loaded Systems

Assessment of Vesicle Size, Polydispersity Index and Zeta Potential

The vesicle size, polydispersity index and zeta potential of the properly diluted aqueous VRD-loaded dispersions were estimated with Zetasizer (Malvern Zetasizer Nano series, Worcestershire, UK), at 25 ± 0.5°C. The dynamic light scattering (DLS) technique investigates the fluctuation in light scattering as a result of the Brownian motion of the particles as function of time, at an angle of 90º.[25]

Estimation of Drug Entrapment Efficiency Percentage (EE%)

The VRD EE% of each system was determined indirectly via the assessment of the unentrapped drug percentage. The

Table 1 The Composition and the Physicochemical Properties of the Investigated Vardenafil Hydrochloride-Loaded Ethosomes; in Comparison to an Aqueous Drug Dispersion; Mean ± SD, n = 3

Systems	* Composition			Physicochemical properties						
	L-α-phosphatidylcholine (mg/mL)	Ethanol (%)	Water (%)	Vesicle Size (nm)	Zeta potential (mV)	[a] EE (%)	[b] $Q_{0.5h}$ (%)	[c] Q_{12h} (%)	[d] Jss (μg. $cm^{-2}h^{-1}$)	Enhancement Ratio (mean)
Drug dispersion			100				8.2±1.4	16.2±3.8	0.2±0.01	1
[e] ETH1	5	20	80	187.5±12.5	-13.5±0.9	70.5±3.0	10.1±0.6	19.6±0.9	0.3±0.02	1.5
ETH2	5	30	70	197.8±21.6	-16.5±0.6	72.3±1.3	12.2±0.7	20.3±1.2	0.6±0.01	3.0
ETH3	5	40	60	192.4±13.5	-14.3±0.5	74.4±0.7	15.1±0.8	25.9±1.8	1.8±0.09	9.0
ETH4	15	20	80	181.3±19.8	-14.3±0.5	73.8±0.3	15.2±0.3	28.2±2.5	1.9±0.07	9.5
ETH5	15	30	70	158.5±17.2	-14.3±0.7	75.3±0.7	17.2±0.7	35.9±2.6	2.7±0.1	13.5
ETH6	15	40	60	172.2±20.9	-15.9±0.7	76.4±1.5	19.8±1.0	46.1±2.4	2.9±0.3	14.5
ETH7	25	20	80	139.1±18.6	-6.34±0.4	74.5±1.6	13.4±0.6	20.5±1.1	1.3±0.05	6.5
ETH8	25	30	70	142.6±15.6	-9.36±0.3	76.9±0.4	15.9±0.4	22.8±1.3	1.2±0.08	6.0
ETH9	25	40	60	137.5±13.3	-17.9±0.8	77.7±1.1	17.6±0.7	43.9±3.2	3.1±0.5	15.5

Note: *All systems contained vardenafil hydrochloride, 5 mg.

Abbreviations: [a]EE%, drug entrapment efficiency percentage; [b]$Q_{0.5h}$, percent drug released after half an hour; [c]Q_{12h}, percent drug released after 12 hours; [d]Jss, steady-state drug flux; [e]ETH (1–9), ethosomal systems (1–9).

Table 2 The Composition and the Physicochemical Properties of the Investigated Vardenafil Hydrochloride-Loaded Invasomes; in Comparison to the Best Achieved Vardenafil Hydrochloride-Loaded Ethosomes; Mean ± SD, n = 3

Systems	* Composition		Physicochemical Properties						
	Limonene (%, v/v)	Cineole (%, v/v)	Vesicle Size (nm)	Zeta Potential (mV)	[a]EE (%)	[b]$Q_{0.5h}$ (%)	[c]Q_{12h} (%)	[d] Jss ($\mu g.cm^{-2}h^{-1}$)	Enhancement Ratio (Mean)
[e]ETH9	–	–	137.5±13.3	−17.9±0.8	77.7±1.1	17.6±0.7	43.9±3.2	3.1±0.5	15.5
[f]ETH9-INV1	0.5		144.5±12.8	−18.3±0.9	79.2±2.6	18.7±0.9	51.6±2.5	3.2±0.2	16.0
ETH9-INV2	1		148.6±19.6	−18.8±0.7	82.3±5.9	16.7±0.7	44.1±2.1	3.5±0.07	17.5
ETH9-INV3	2		155.8±22.6	−19.1±1.3	85.7±9.7	15.3±1.0	47.5±2.3	3.3±0.2	16.5
ETH9-INV4		0.5	139.3±10.9	−18.7±0.8	78.5±7.1	18.5±1.1	36.8±1.8	4.1±0.1	20.5
ETH9-INV5		1	151.1±21.6	−19.5±1.7	88.6±1.9	21.4±0.9	45.8±2.2	4.5±0.5	22.2
ETH9-INV6		2	163.8±13.9	−21.3±1.9	89.4±4.5	9.5±0.4	42.6±1.2	4.8±0.1	24.0
ETH9-INV7	0.25	0.25	140.7±12.4	−18.8±0.9	79.7±1.6	27.6±1.3	72.1±3.6	5.7±0.2	28.5
ETH9-INV8	0.5	0.5	159.9±24.9	−20.3±1.1	81.3±3.7	25.4±1.2	85.3±4.2	6.4±0.3	32.0
ETH9-INV9	1	1	172.5±30.8	−20.9±1.8	88.5±2.8	22.2±1.1	72.9±3.6	5±0.1	25

Note: *In addition, all systems contained vardenafil hydrochloride (5 mg), L-α-phosphatidylcholine (25 mg), ethanol (40%) and water (60%).
Abbreviations: [a]EE%, drug entrapment efficiency percentage; [b]$Q_{0.5h}$, percent drug released after half an hour; [c]Q_{12h}, percent drug released after 12 hours; [d]Jss steady-state drug flux; [e]ETH9, ethosomal system 9; [f]ETH9-INV (1–9), ethosomal system 9-derived invasomal systems (1–9).

VRD-loaded dispersion was centrifuged at 15,000 rpm (1 h; 4°C) (Heraeus Megafuge® 1.0 R; Hanau, Germany) and the clear supernatant was properly diluted. The free VRD concentration was assessed spectrophotometrically at 250 nm.[16] The VRD EE% was calculated according to Eq. (1)

$$\%EE = \frac{\text{Total theoratical drug content(mg)} - \text{unentrapted drug content(mg)}}{\text{Total theoratical drug content(mg)}} X100 \quad (1)$$

Ex vivo Drug Permeation Studies

The ex vivo drug permeation studies were carried out according to the guidelines of Research Ethics Committee of Faculty of Pharmaceutical Sciences and Pharmaceutical Industries, Future University in Egypt (FUE) (Approval No. REC-FPSPI-7/47). Male Wistar rats (200–250 g) were euthanized with an overdose of sodium thiopental. The dorsal hair was removed by shaving with an electric shaver. The full-thickness skin was extracted and inspected for scratches, bites or any abnormalities. The subcutaneous fats were carefully removed, so that the epidermis layers were kept intact. The skin samples were stored at –20°C and were used within 3 days of skin harvest. Prior to testing, the skin samples were allowed to thaw and were left to equilibrate at room temperature in phosphate buffer saline (pH 7.4, 24 h) to maintain a trans-epidermal hydration gradient. Following, the samples were carefully mounted between the donor and the receptor compartments of the Franz diffusion cells (Hanson research, Vision® Microette™ automated diffusion test system, Chatsworth, CA) with the stratum corneum side up. The permeation surface area was 1.767 cm^2 and the stirring rate was adjusted at 600 rpm. The receptor medium was loaded with phosphate buffer saline (pH 7.4, 7.2 mL) and the temperature was maintained at 32 ± 0.5°C.[26,27] One-mL samples of the investigated system dispersions, containing the equivalent of 5 mg of VRD, were loaded into the donor compartments. Aliquots of the receptor compartments were collected and replenished with fresh medium via the autosampler at 0.5, 1, 2, 4, 8 and 12 hrs. The cumulative drug permeated percentages per unit surface area were plotted as a function of time. Control experiments were similarly conducted using an aqueous drug dispersion; 5 mg/mL. For comparison, the cumulative drug permeated percentages after 0.5hrs ($Q_{0.5h}$) and 12hrs (Q_{12h})[28] as well as the steady-state flux (Jss) of each system were estimated. Jss was calculated from the linear portion of each curve, according to Eq. 2.

$$J_{ss} = \frac{\text{Amount of drug permeated}}{\text{Time} \times \text{Areaofskin}} \quad (2)$$

The enhancement ratio (Er) was calculated by dividing Jss of each test treatment by that of the control treatment. Statistical comparison was performed using one-way analysis of variance (ANOVA) test at a P value of 0.05.

The aliquots were analyzed via HPLC, at 250 nm, according to the method of Carlucci et al,[29] with a slight modification. The mobile phase, consisting of phosphate buffer saline (pH 7.4) and acetonitrile (70:30), was adjusted to flow at a rate of 1 mL/min in an isocratic elution mode. The HPLC system consisted of Shimadzu chromatographic system (Kyoto,

Japan) equipped with Shimadzu LC-10 AD VP pump, DGU-12A degasser and SCL-10A VP system controller. Samples were injected using Spectra System Auto sampler AS4000 at an injection volume of 20 µL. The chromatographic separation was performed on Waters C_{18} column (µBondpak, 125A°, 10 µm, 4.6 mm ×250 mm). A calibration curve ($R^2 = 0.995$) was constructed by plotting the peak area against drug concentration. The procedural constant was calculated from the slope of the curve.

Selection of the Best Achieved VRD-Loaded Ethosomal System

The data were statistically analyzed to select the best achieved ethosomal system which possesses the highest desirability value; with respect to five constraints. The vesicle size and $Q_{0.5h}$ were targeted to be at minimum while the EE%, Q_{12h} and Jss values were aimed to achieve maximum values. The best achieved ethosomal system was further optimized to various invasomal systems via the incorporation of terpenes.

Morphologic Examination

The morphologic examination of the optimized VRD-loaded ethosome-derived invasomes (ETH9-INV8) was conducted to examine the vesicular structural attributes like the uniformity of shape and size and explore the presence of aggregates. Briefly, one drop of the properly diluted aqueous dispersion was deposited onto the surface of a 300-mesh carbon-coated copper grid and was allowed to settle for 3–5 min. The excess fluid was removed and left to dry, at room temperature, prior to investigation via Transmission Electron Microscope (JEM 1230, Tokyo, Japan) at 80 kV under a magnification power of 80,000 X.

Skin Irritation Studies

The histopathologic studies of the optimized VRD-loaded ethosome-derived invasomes (ETH9-INV8) were evaluated in rats to explore their possible skin irritation potential. Six rats were enrolled in the studies and were divided into two equal groups. The first group were treated with saline solution (control treatment), while the second group were treated with the optimized system (test treatment). Twenty-four hours prior to testing, the animals' backs were shaved and were allowed to rest overnight. On the study day, one-mL samples were carefully rubbed on each rat. Following a leave-on period of 12 h, the animals were sacrificed. Skin biopsies were derived, fixed in 10% (v/v) formol saline solution for 24 h, washed in warm water and finally treated with methyl alcohol, ethyl alcohol and absolute ethyl alcohol for dehydration. Tissue specimens were embedded in paraffin, sectioned, loaded onto glass slides, deparaffinized, stained (hematoxylin and eosin) and finally examined microscopically.[30]

Confocal Laser Scanning Microscopy (CLSM) Studies

CLSM examination was conducted using a fluorescent dye, rhodamine B. The dye was incorporated (0.1% w/v) into the optimized VRD-loaded ethosome-derived invasomes (ETH9-INV8). For the control treatment, the dye was loaded, at a similar concentration, into VRD-loaded hydroalcoholic solution (40%, v/v). The investigated treatments were added to the donor compartments of the Franz diffusion cells over the epidermal skin surfaces for 4 h. Following, the skin samples were removed, rinsed with distilled water, and fixed for 24 h.[17,31] The samples were vertically cross-sectioned into pieces and were examined via Zeiss LSM 510-META inverted confocal laser scanning microscope (Carl Zeiss, Jena, Germany).

PBPK Modeling Approach

For verification of the investigated modeling software, the pharmacokinetic parameters of VRD (C_{max}, T_{max} and $AUC_{0\text{-}24h}$) following the oral administration of a single 20 mg dose, after over-night fasting, were predicted and compared to the reported clinical data by Stark et al.[32]

The estimation of the pharmacokinetics of VRD following the transdermal application of the best achieved ETH9-INV8 system, relative to an aqueous drug dispersion, in adults and geriatrics was based on the current ex vivo drug permeation data as well as the input data, listed in Table 3, for VRD.[33–36] The drug dose in both treatments was fixed at 5 mg.

Results and Discussion

Development of VRD-Loaded Ethosomes

The current work aimed to develop and optimize a promising VRD-loaded vesicular systems which are able to overcome the limitations associated with oral drug administration, enhance its bioavailability and offer a non-invasive transdermal delivery system which could be used for patients suffering from PAH. As reported by Abdulbaqi et al,[37] for ethosomes, the optimum ethanol concentrations vary from 20 - 40% (v/v). At lower concentrations, the drug EE% will be minimal. Whereas, ethosomal membranes will be more permeable at very high concentrations because PC can easily be dissolved in ethanol, leading to a significant reduction in drug EE%. In our preliminary studies, it was proved that higher PC concentrations (beyond 25 mg/mL; 2.5% w/v) had

Table 3 The Input Data Required for Building a Physiologically Based Pharmacokinetic Model for Predicting the Transdermal Delivery of Vardenafil Hydrochloride

Parameters	Value	Reference
Molecular weight (g/mol)	579.1	[33]
[a]pKa_1	3.4	[33]
[a]pKa_2	6.7	[33]
[a]pKa_3	8.8	[33]
[b]Cl (L/h)	56	[33]
[c]Log P	2.65	[34]
[d]R_b	0.81	[35]
[e]Cl_{int} rCYP3A4 (mL/min/pmol)	2.8	[36]
[f]Cl_{int} rCYP3A5 (mL/min/pmol)	18	[36]

Notes: [a]Dissociation constants of drug; [b]total body clearance; [c]partition coefficient; [d]blood to plasma concentration ratio; [e]intrinsic clearance of cytochrome P450 CYP3A metabolized drug measured in recombinant CYP3A4; [f]intrinsic clearance of cytochrome P450 CYP3A metabolized drug measured in recombinant CYP3A5.

no significant influence on drug EE%. Therefore, the response surface design was employed to study the influence of PC concentration (5, 15 and 25 mg/mL) and ethanol percentage (20%, 30% and 40% v/v) on the characteristics of VRD-loaded ETHs. Nine systems were simply developed via the ethanol injection technique. This was followed by homogenization to promote the development of finer dispersions.

Characterization of VRD-Loaded Ethosomes

Assessment of Vesicle Size, Polydispersity Index and Zeta Potential

The vesicle size of the investigated ETHs ranged from 137.5 ± 13.3 nm (ETH9) to 197.8 ± 21.6 nm (ETH2). The PDI values (not shown) were in the range of 0.174 to 0.258. This could reveal the development of uniform nanovesicles which are characterized by narrow size distributions; Table 1.

At a constant ethanol%, an indirect correlation was statistically ($P< 0.05$) revealed between the PC concentration and the mean vesicle size. The decrease in mean vesicle size at high PC concentrations could be related to the reduction in the interfacial tension between the water and lipid phases, resulting in the formation of vesicles of lower size. Furthermore, high PC concentrations could adequately stabilize the vesicles by establishing steric barriers on their surfaces and thereby, protect them from coagulation. These results agree with Vikbjerg et al,[38] who studied the emulsifying properties of different phospholipids and reported a negative correlation between PC concentration and the vesicle size. At a fixed PC concentration, ethanol showed a non-significant ($P< 0.05$) influence on the mean vesicle size. It is worth noting that the smallest vesicle size (137.5 nm) was revealed with ETH9 system containing the highest PC concentration and the largest ethanol percentage. Ethanol was suggested to considerably decrease the thickness of the vesicle membrane due to the interpenetration of its hydrocarbon chain into the vesicular lipid bilayers. Moreover, it provides a steric stabilization which could result in a vesicular size reduction.[39]

The zeta potential values of ETHs are listed in Table 1. All systems showed negative values ranging from −6.34 ± 0.4 mV (ETH7) to −17.9 ± 0.8 mV (ETH9). These results were in line with those reported by Iizhar et al,[40] who developed terbinafine hydrochloride-loaded ethosomes possessing negative zeta potential values varying from −7.10 mV to −7.96 mV. The synergistic influence of ethanol and PC on the magnitude of the negative charge of ETH9 system should be considered. According to Limsuwan et al,[41] the incorporation of a high ethanol percentage (40%, v/v) in the system would augment the negative charge stabilization on the vesicles due to the electrostatic repulsions and the subsequent de-aggregation. In a parallel line, the enrollment of PC at a high concentration (25 mg/mL) would add to the zeta potential value.[42] It was postulated that in a medium of low ionic strength, the polar head group is directed in a manner that the negatively charged phosphatidyl group is oriented to the outside while the positively charged choline group is positioned to the inside, leading to a net negative charge on the surface.[43,44]

Estimation of VRD Entrapment Efficiency%

The drug EE% of VRD varied from 70.5 ± 3.0% (ETH1) to 77.7 ± 1.1% (ETH9); Table 1. These promising drug entrapment efficiency percentages could be attributed to the capability of ETHs to accommodate the drug.[45] At a fixed ethanol%, a direct correlation was revealed between PC concentration and VRD EE%. According to Tadros and Al-mahallawi,[46] this could be explained with respect to the surface-active properties of lecithin which would promote the development of strong coherent layers surrounding the individual vesicles, and thus can minimize the escape of the drug. At a constant system volume, a higher system viscosity would be expected at a higher PC concentration. This could be expected to retard the external diffusion of the drug.[47] The positive contribution of ethanol% on VRD EE% could be related to the enhanced solubility of VRD in ethanol.[48]

Ex vivo Drug Permeation Studies

The ex vivo drug permeation data from VRD-loaded ETHs, in comparison to an aqueous VRD dispersion, are summarized in Table 1 and are graphically represented in Figure 1. All systems showed significantly ($P< 0.05$) higher $Q_{0.5h}$, Q_{12h} and J_{ss} values compared to VRD dispersion, suggesting their enhanced transdermal abilities. The $Q_{0.5h}$ percentages ranged from 10.1 ± 0.6% (ETH1) to 19.8 ± 1.0% (ETH6), while the Q_{12h} percentages varied between 20.3 ± 1.2% (ETH2) and 46.1 ± 2.4% (ETH6). As for J_{ss}, the highest value (3.1 ± 0.5 $\mu g.cm^{-2}h^{-1}$) and consequently, the highest enhancement ratio (15.5) was achieved with ETH9 system (Table 1).

At a constant ethanol%, a direct correlation was statistically ($P< 0.05$) revealed between PC concentration and drug permeation parameters ($Q_{0.5h}$, Q_{12h} and J_{ss}). The penetration enhancing effect of PC is initiated by its high affinity to the epidermis and by its ability to fluidize the lipid components of the skin.[49–51] This correlation held true till a PC concentration of 15 mg/mL. Except for ETH9, a further increase in PC concentration had significantly ($P< 0.05$) reduced the values of the drug permeation parameters. This could be attributed to the firmer state of the lipid membrane at higher PC concentrations. According to Kriwet and Müller-Goymann,[52] the lowering in drug release percentages with higher PC concentrations could be related to the higher affinity of hydrophobic drugs, like VRD, to the vesicles' bilayers. Furthermore, the lowering in the thermodynamic activity of VRD and the subsequent higher drug EE% within vesicles which possess higher PC concentrations should also be considered.

At a fixed PC concentration, a direct correlation was statistically ($P< 0.05$) revealed between ethanol% and the drug permeation parameters. This correlation may be traced to the dual effect of ethanol on the lipid bilayers in the stratum corneum as well as in the ETHs. Ethanol fluidizes PC bilayers forming compact, deformable, and soft ethosomes. In a parallel line, it interacts with the polar head in the lipid region of SC, allowing for a possible reduction in the transition temperature and an increase in the membrane fluidity.[53,54]

Based on the set constraints for vesicle size, drug EE%, $Q_{0.5h}$, Q_{12h} and J*ss* values, one system (ETH9), which possessed the highest desirability value (0.91), was promoted for further optimization studies.

Development of VRD-Loaded Invasomes

In the last years, several reports demonstrated the advantages of invasomes as a promising vesicular system; with regards to ease of formulation, high flexibility and stability, enhanced drug permeation capability as well as improved drug bioavailability.[55–58] In the present work, the best achieved VRD-loaded ETH9 system was

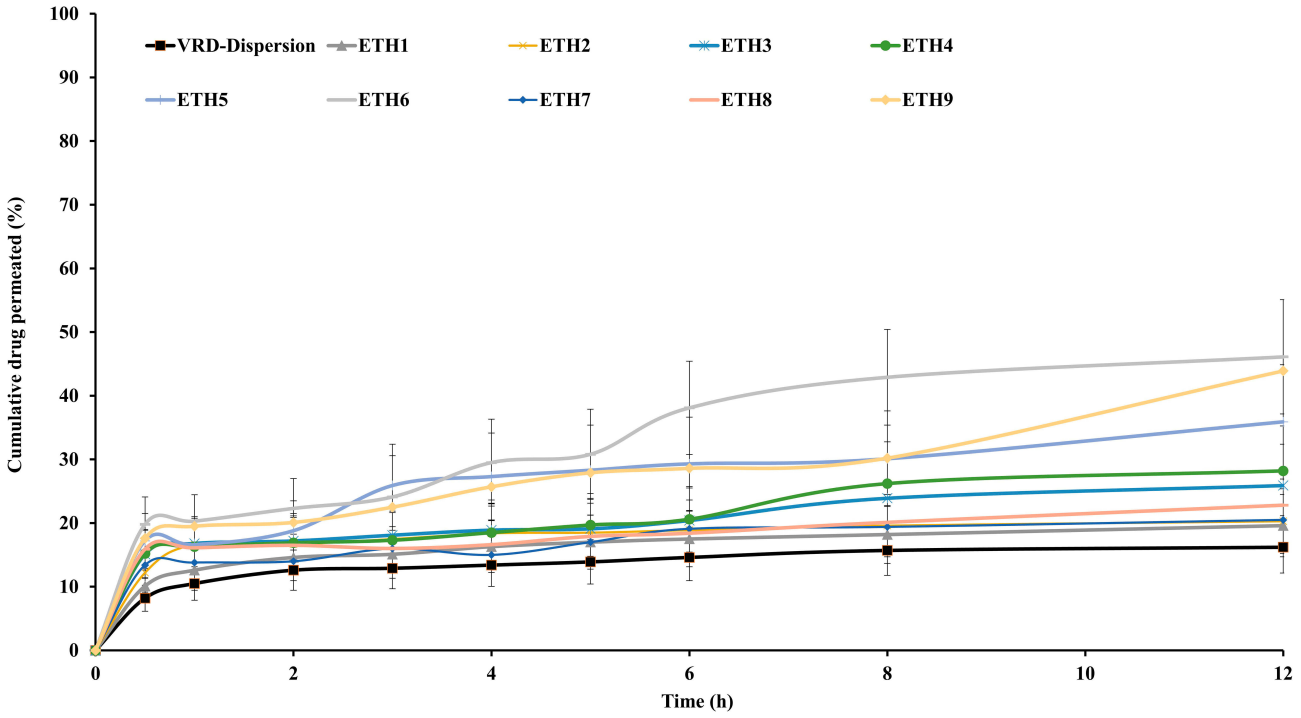

Figure 1 The ex vivo drug permeation profiles from vardenafil hydrochloride-loaded ethosomal systems, in comparison to an aqueous vardenafil dispersion.

optimized to various invasomal systems via incorporation of limonene, cineole or a 1:1 mixture of limonene and cineole at 0.5%, 1% or 2% v/v.

Characterization of VRD-Loaded Invasomes

The vesicle size distribution of VRD-loaded INVs varied from 139.3 ± 10.9 nm (ETH9-INV4) to 172.5 ± 30.8 nm (ETH9-INV9); Table 2. Compared to ETH9, the incorporation of terpenes led to an increase in the size of the vesicles. This finding agreed with that reported by Dragicevic-Curic et al,[55] for the presence of a direct correlation between the terpene concentration and the vesicle size.

The PDI of the investigated VRD-loaded INVs was in the range from 0.291 to 0.410 (data not shown), indicating the development of partially homogeneous vesicular systems.

Compared to the zeta potential value of VRD-loaded ETH 9 (−17.9±0.8), the zeta potential values of VRD-loaded INVs were higher, ranging from −18.3 ± 0.9 mV (ETH9-INV1) to −21.3 ± 1.9 mV (ETH9-INV6); Table 2. It could be inferred that the incorporation of terpenes in VRD-loaded INVs would potentiate the effect of ethanol and hence, increase the magnitude of negative charge. This influence is expected to promote the electrostatic repulsion, prevent the aggregation of vesicles and promote the physical stability of the developed INVs.[55]

Compared to the EE% of VRD-loaded ETH9 (77.7 ±1.1%), the EE% of the developed VRD-loaded INVs were larger, varying from 78.5±7.1% (NE9-INV4) to 89.4±4.5% (NE9-INV6); Table 2. The existence of a direct correlation between the terpene concentration and VRD EE% was elucidated. During the development of INVs, the lipophilic terpene was dissolved, along with PC, in ethanol. The acyl chains of PC would produce a good environment for the incorporation of terpene and VRD within the vesicular bilayers. The higher the terpene concentration, the greater the lipophilicity. This would promote higher solubilization of VRD in the bilayers and hence, higher VRD EE% would be expected.[59] The ex vivo permeation data of VRD from VRD-loaded INVs, in comparison to VRD-loaded ETH9, are summarized in Table 2 and are graphically illustrated in Figure 2. Higher transdermal flux values, ranging from 3.2 ± 0.2 $\mu g.cm^{-2}h^{-1}$ (ETH9-INV1) to 6.4 ± 0.3 $\mu g.cm^{-2}h^{-1}$ (ETH9-INV8), were revealed with VRD-loaded INVs. Statistical analysis of the J_{ss} values revealed the superiority of the systems containing a mixture of limonene and cineole over their corresponding systems prepared using either cineole or limonene.

A direct correlation was observed between the concentration of limonene and J_{ss} values. This correlation was held

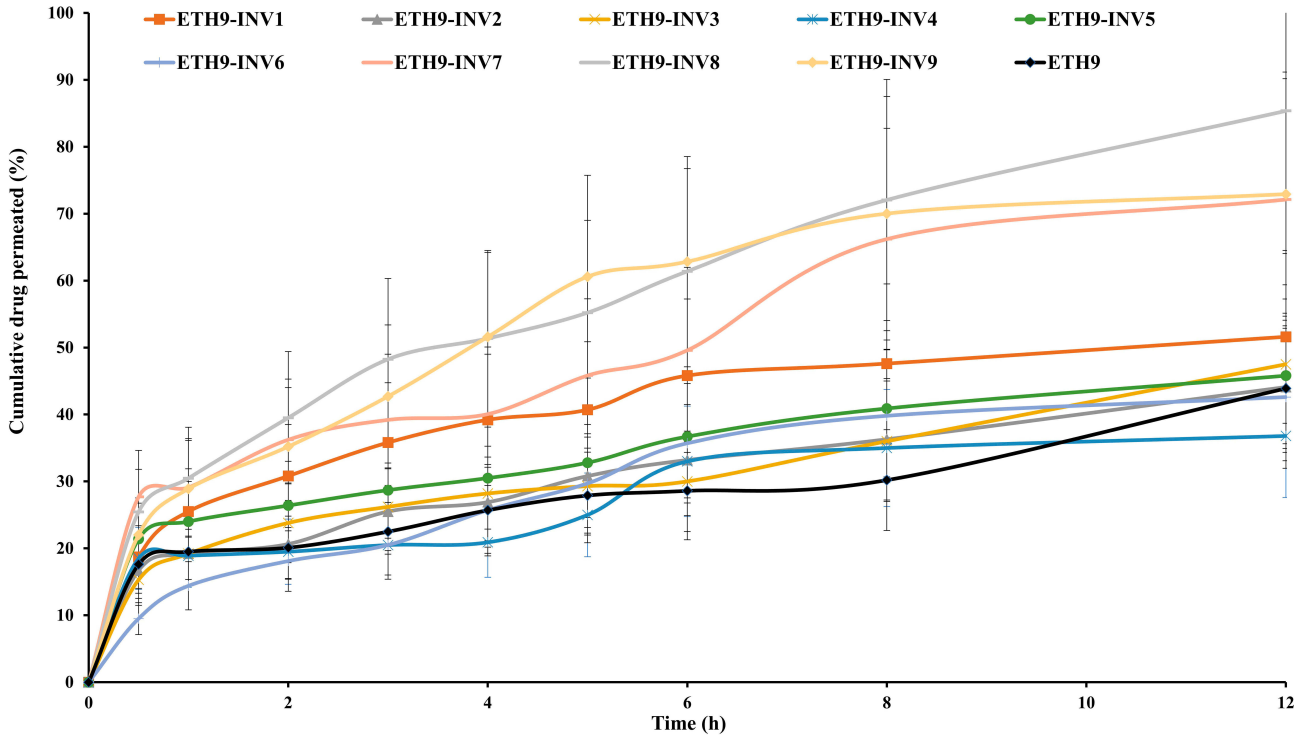

Figure 2 The ex vivo drug permeation profiles from vardenafil hydrochloride-loaded invasomal systems, in comparison to the best-achieved vardenafil hydrochloride-loaded ethosomal system.

true till a limonene concentration of 1%. Beyond which, the J_{ss} value decreased. A similar pattern was reported for estradiol following the incorporation of limonene into PC-based liposomes. A subsequent lowering in the transdermal flux was revealed with the further increase in limonene concentration. This pattern was attributed to the development of one or more new species at high limonene concentrations, as revealed via a highly sensitive differential scanning calorimetry study.[60] According to Zhao and Singh,[61] the permeation enhancing effect of a mixture of limonene/ethanol on propranolol hydrochloride could be related to macroscopic barrier perturbation, lipid extraction from SC and the enhancement in the drug partitioning to SC.

Many ceramides are arranged in a tight manner via hydrogen bonding within SC lipid bilayers. The hydrogen bonding makes the lipid bilayers stable, strong and be able to maintain the barrier merit of SC. In the current work, the concentration-dependent enhancement effect of cineole on J_{ss} could be related to its ability to lower the amide-I stretching frequency and break the intra- and inter-lamellar hydrogen-bonding networks. The structure of cineole contains an ether group which could facilitate the formation of hydrogen bonding in skin ceramides via the free oxygen.[62,63]

Of the investigated systems, significantly ($P< 0.05$) higher Q_{12h} (85.3 ± 4.2%) and higher flux (6.4 ± 0.3 $\mu g.cm^{-2}h^{-1}$) were achieved with ETH9-INV8 system which contains a 1% terpene mixture of limonene and cineole. Interestingly, significantly ($P< 0.05$) lower Q_{12h} (72.9 ± 3.6%) and lower flux (5 ± 0.1 $\mu g.cm^{-2}h^{-1}$) were attained upon increasing the concentration of the terpene mixture. This could be ascribed to the greater solubilization of VRD. The subsequent lowering in the thermodynamic activity of the drug would be expected to reduce the values of drug permeation parameters. One should consider that the increase of terpene concentration might lead to dehydration of the SC.[64] These findings match with those reported by Kunta et al,[65] for the enhanced transdermal permeation of propranolol up to a certain terpene concentration with no added value at higher concentrations.

Based on the achieved values of particle size, EE%, $Q_{0.5h}$, Q_{12h} and J_{ss} for the investigated systems and the subsequent estimation of their desirability values, one optimized invasomal system (ETH9-INV8) was promoted for further characterization studies.

Characterization of the Optimized VRD-Loaded Invasomes

A representative TEM micrograph of ETH9-INV8 is illustrated in Figure 3. The development of spherical vesicles was revealed. They appear to have a lower vesicle size than that revealed via DLS (Table 2). This could be explained with respect to the possible aggregation of some vesicles during DLS measurements.

The light microscopic examination of rat skin samples which were treated with normal saline solution revealed the presence of normal skin architecture which is characterized with well-defined epidermis, dermis, and subcutaneous tissue with sebaceous glands and hair follicles (Figure 4A). In a parallel line, no signs of skin irritation (like erythema or edema) were visually observed during the application of the optimized ETH9-INV8 system for 12hrs. Microscopically, minor histopathologic changes were revealed. This could indicate a promising safety and good skin biocompatibility (Figure 4B).

The CLSM studies were conducted to explore the skin permeation ability of the optimized invasomal system (ETH9-INV8) after 12hrs, compared to VRD-loaded hydroalcoholic solution. The control treatment showed slight distribution of the dye (green fluorescence) over the SC. Very low intensities were revealed at the subsequent skin layers (Figure 5A). On the other hand, the invasomal system was deposited over the SC, the epidermis and the hypodermis layers with higher fluorescence intensities (Figure 5B). It could be inferred that the incorporation of ethanol was not the only driving force for promoting effective drug permeation via skin. One could speculate the synergistic effect of PC, ethanol and terpenes. Traditionally, three skin permeation pathways are identified viz., through-corneocytes as a transcellular route, between-corneocytes as a paracellular route, and through appendages.[66] Dragicevic-Curic et al[55] suggested that some invasomes might break up during permeation in the upper skin layers. Hence, PC and terpenes are retained where they can change the transition temperature, fluidize the intercellular lipids and allow the drug to permeate into deeper skin layers. In parallel, the ethanol content in smaller invasomes can similarly fluidize the intercellular lipids and enhance their flexible intact permeation via the hair-follicles and/or the narrow hydrophilic channels distributed within the intercellular lipids. The follicular ducts contain lipophilic sebum secretions derived from the sebaceous glands. The apparent intense fluorescence near the hair follicles could be referred to the localized accumulation of the developed lipophilic vesicles.[66] Based on these findings, the follicular pathway could be described as the main skin permeation route for VRD-loaded invasomes. Since the hair follicles are surrounded by blood

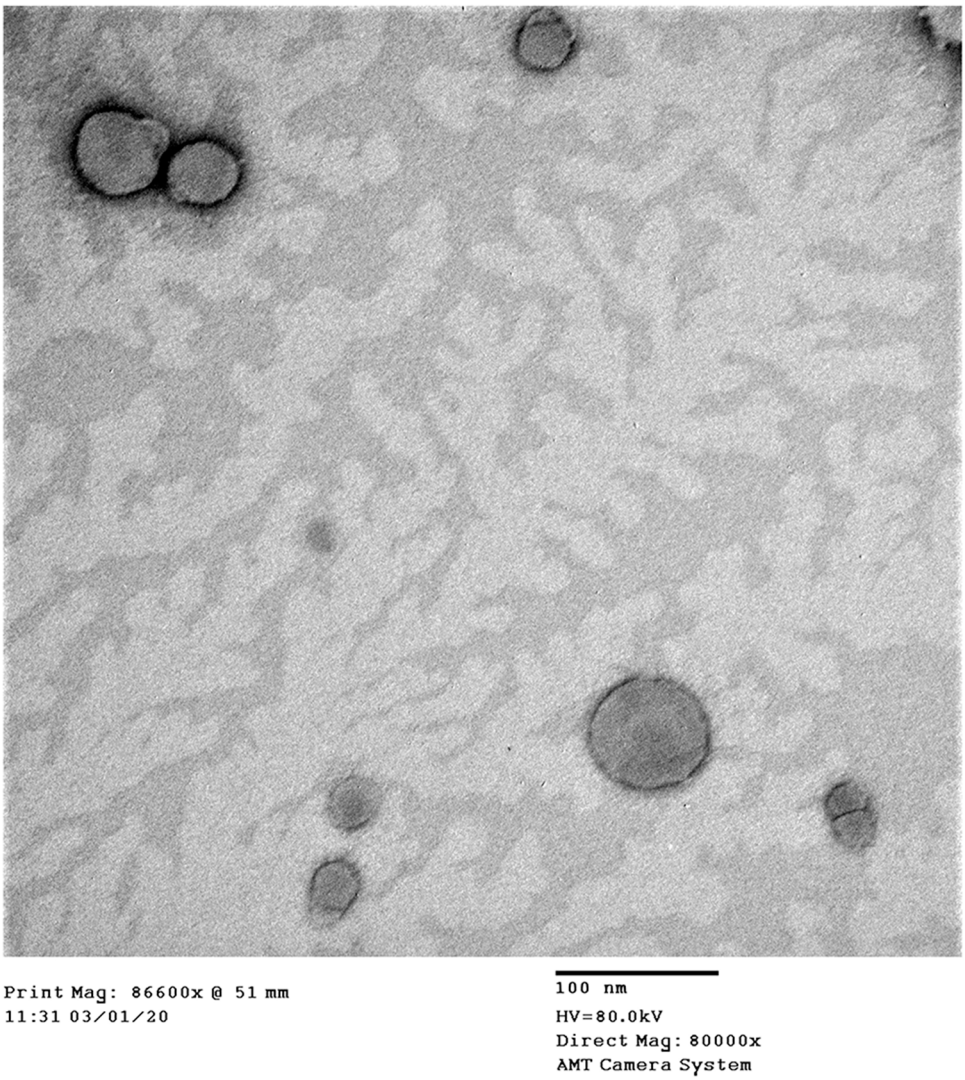

Figure 3 A representative transmission electron micrograph of ETH9-INV8 system [ethosomal system 9-derived invasomal system 8].

capillaries, then the drug-loaded systems would be expected to deeply permeate the skin layers and reach the systemic circulation as micro-reservoir systems which are able to sustain the rate of drug release and/or improve its bioavailability by avoiding the first-pass effect.

Analysis of the Results of PBPK Model

Prior to the prediction of the pharmacokinetic parameters of VRD in human volunteers following the transdermal application of the optimized ETH9-INV8 system, the investigated PBPK model should be verified against the reported clinical data. The verification of the model was achieved by comparing PBPK model-simulated (predicted) pharmacokinetic parameters (T_{max}, C_{max}, and $AUC_{0\text{-}24h}$) of VRD following a single oral dose of 20 mg to the corresponding reported pharmacokinetic parameters by Stark et al,[32] Table 4. It was revealed that mean predicted/observed ratios for T_{max}, C_{max}, and $AUC_{0\text{-}24h}$ were 1.06, 0.98 and 0.82, respectively. This could confirm the validity of the investigated modelling software and the adopted model.

The PBPK model-simulated plasma concentration–time curves of VRD following the transdermal application of ETH9-INV8 system in adults and geriatrics, relative to an oral aqueous drug dispersion, are portrayed in Figure 6. The predicted pharmacokinetic parameters are summarized in Table 5.

For adults, the mean C_{max} value of the drug following the transdermal application of ETH9-INV8 system (2.3 µg/L) was lower than the corresponding mean value (4.8 µg/L) achieved with the aqueous drug dispersion. An accelerated absorption rate was observed by the latter as illustrated by the steep mountain-like appearance in the plasma concentration-

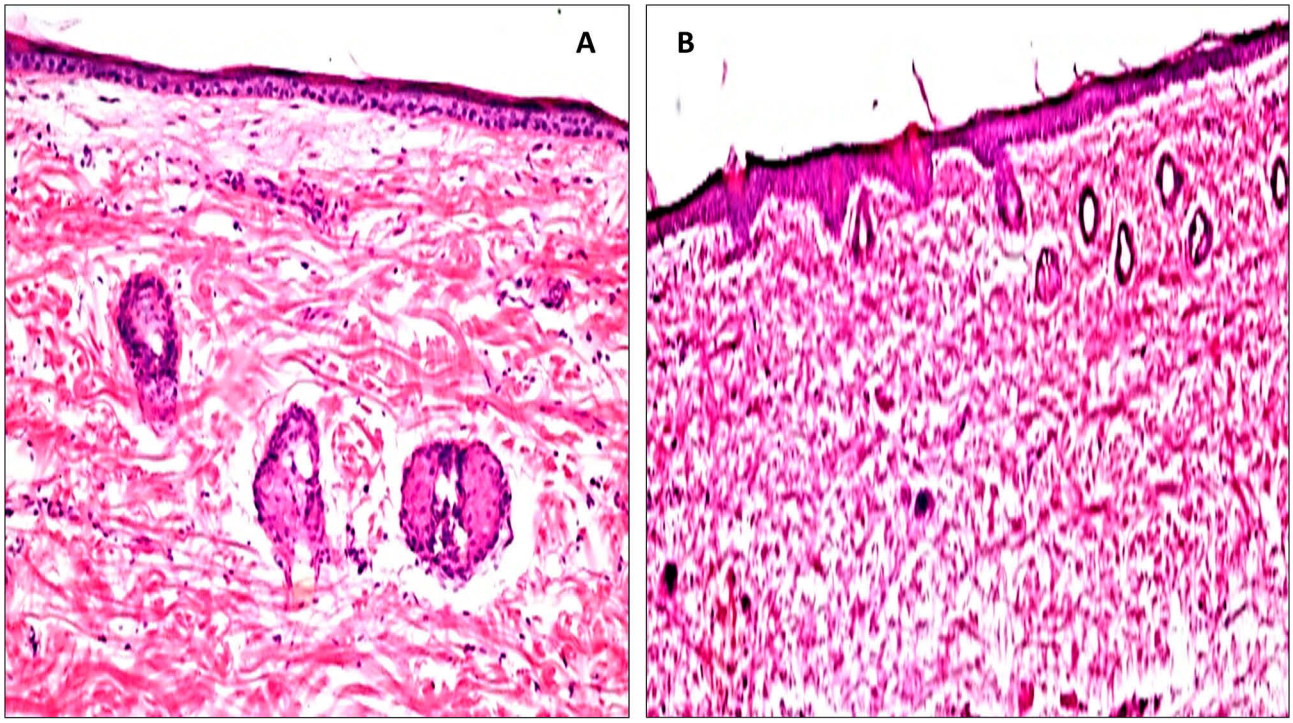

Figure 4 Histopathologic micrographs of hematoxylin and eosin-stained rat skin samples treated with normal saline solution (**A**) and ETH9-INV8 system [ethosomal system 9-derived invasomal system 8] (**B**).

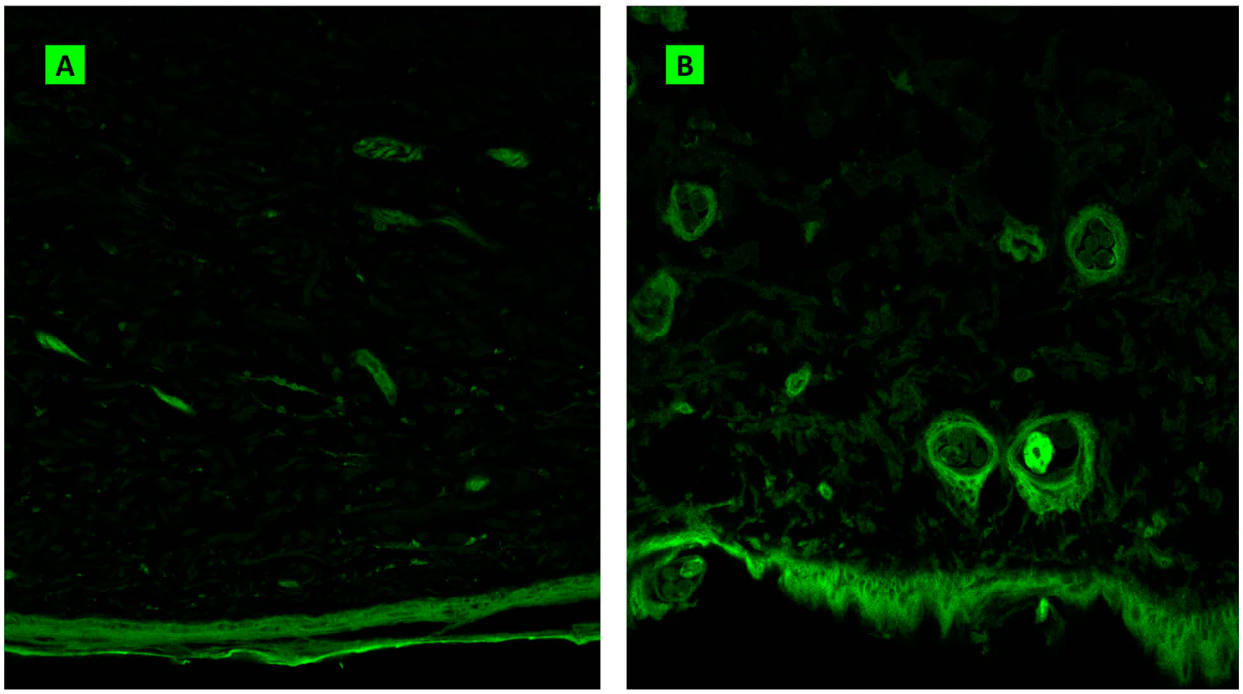

Figure 5 Confocal laser scanning micrographs of rat skin samples treated withvardenafil hydrochloride-loaded hydroalcoholic solution (**A**) and ETH9-INV8 system [ethosomal system 9-derived invasomal system 8] (**B**).

time plot. It was clear that the maximum drug concentration descended rapidly to markedly lower concentrations. The drug plasma concentration–time curve following oral drug administration showed a pattern that can be generalized, with subsequent doses, as peaks and troughs. On the other hand, an almost steady-state drug plasma concentration–time curve

Table 4 Comparison of Physiologically Based Pharmacokinetic Model Simulated (Predicted) and Clinical (Observed) Vardenafil Hydrochloride Pharmacokinetic Parameters Following a Single Oral Dose of 20 Mg (n = 21 in Observed Data and n = 100 in Predicted Data)

Treatment Dose of 20 mg	[a]T_{max} (h)	[b]C_{max} (μg/L)	[b]$AUC_{0\text{-}24h}$ (μg.h/L)
Predicted data	0.7 (0.5–1.2)	19.0 ± 11.5	56.0 ± 36.0
[c]Observed data	0.66 (0.25–2.58)	19.30 ± 1.71	68.00 ± 1.76
Mean predicted/observed ratio	1.06	0.98	0.82

Table 5 Physiologically Based Pharmacokinetic Model Simulated Vardenafil Hydrochloride Pharmacokinetic Parameters Following Transdermal Application of ETH9-INV8 System and an Oral Drug Dispersion, at 5 Mg Doses, in Adults and Geriatrics (n = 100)

Treatment Dose of 5 mg	Population	[a]T_{max} (h)	[b]C_{max} (μg/L)	[b]$AUC_{0\text{-}24h}$ (μg.h/L)
Oral drug dispersion	Adults	0.7 (0.5–1.3)	4.8 ± 2.8	14.0 ± 9.0
	Geriatrics	0.7 (0.5–1.1)	5.9 ± 3.7	20.1 ± 13.6
Transdermal ETH9-INV8	Adults	2.8 (2.1–12.0)	2.3 ± 0.9	30.6 ± 11.5
	Geriatrics	3.2 (2.2–24.0)	2.3 ± 0.9	34.1 ± 13.6

Notes: [a]Median (range); [b]mean ± standard deviation; [c]observed data as retrieved from Stark et al.[32]
Abbreviations: ETH9-INV8, ethosomal system 9-derived invasomal system 8; T_{max}, time-to-maximum drug concentration; C_{max}, maximum drug concentration; $AUC_{0\text{-}24h}$, area under the time–concentration curve.

was revealed following the transdermal application of ETH9-INV8 system. This pattern would promote prolonged drug delivery to those patients suffering from PAH. The respective median T_{max} values of VRD following oral administration of an aqueous drug dispersion and the transdermal application of ETH9-INV8 system were 0.7 h and 2.8 h. The shorter T_{max} of the former treatment may be attributed to the rapid oral absorption of VRD from the GIT into the systemic circulation. On contrary, the delayed T_{max} value of the later could be related to the barrier function of the SC and the multilayer

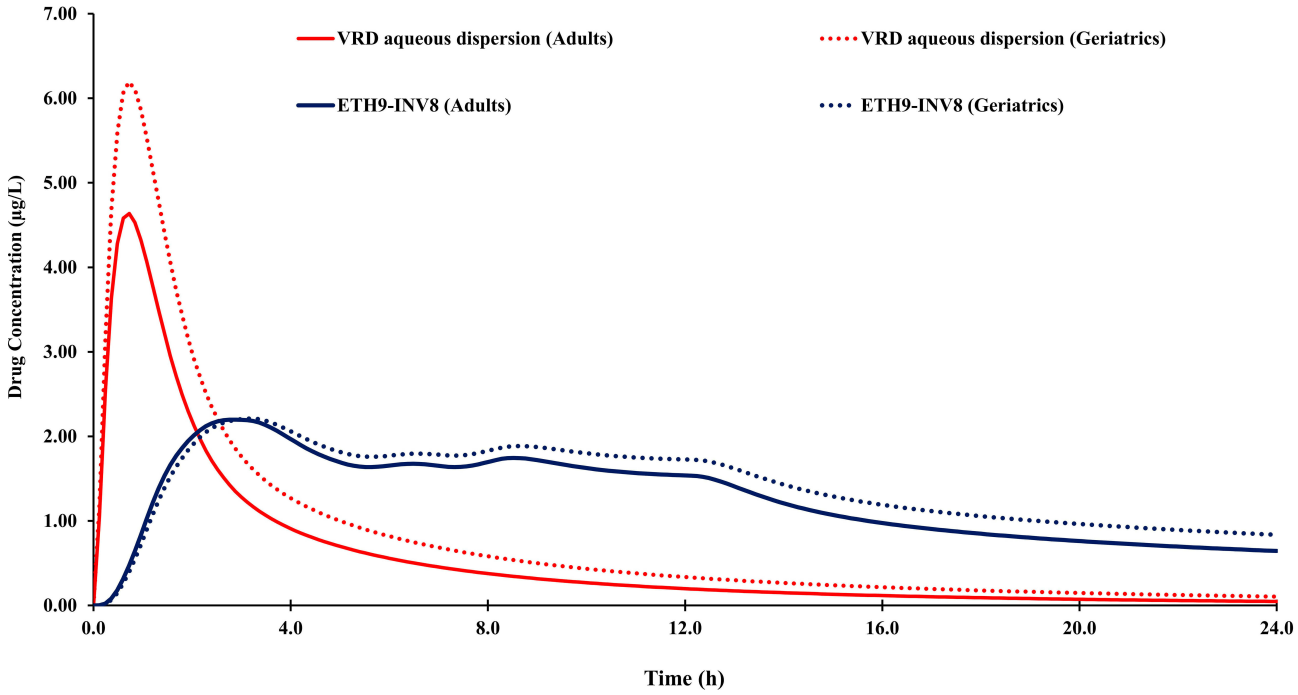

Figure 6 Physiologically based pharmacokinetic model simulated vardenafil hydrochloride plasma concentration–time curves following transdermal application of ETH9-INV8 system [ethosomal system 9-derived invasomal system 8] and an oral drug dispersion, at 5 mg doses, in adults and geriatrics.

structure of the skin which retards the rapid drug diffusion into the systemic circulation. As revealed via CLSM studies, the system is expected to deeply permeate the skin layers and reach the systemic circulation as micro-reservoir systems which can sustain the rate of drug release. Based on the mean $AUC_{0\text{-}24h}$ values of the control (14.0 µg.h/L) and the test treatment (30.6 µg.h/L), the relative drug bioavailability would be 218.57%. The boosted bioavailability could be attributed to a number of factors, including (i) the lipophilic nature of VRD, (ii) the synergistic effect of PC, ethanol and terpene mixture for enhancing the drug permeation into deep skin layers and (iii) the small vesicle size of the system. The high surface area/volume ratio would allow a facilitated contact between the system and the skin. One should consider that promising transdermal systems, which are able to deliver an almost steady-state drug concentrations, are beneficial to lower the side-effects of the drug which are commonly elaborated with immediate release systems.

Significant changes in the body physiology occur with advancing age. Aging involves progressive impairments in the functional reserve of many organs, which might also affect drug metabolism and pharmacokinetics. Lipophilic drugs may have an increased volume of distribution with a prolonged half-life due to the reduction in the glomerular filtration rate.[67] The hepatic first-pass effect of the highly cleared drugs could be reduced due to the progressive reduction in the liver mass and in the blood perfusion. Hence, the bioavailability of such drugs can be increased in the elderly.[68] The PBPK model-simulated pharmacokinetic parameters of VRD following oral administration of an aqueous drug dispersion in geriatrics revealed a higher mean C_{max} value (5.9 ± 3.7 µg/L). Within the same population, the median T_{max} value of VRD following the transdermal application of ETH9-INV8 system was more delayed (3.2 h vs 0.7 h). Based on the respective mean $AUC_{0\text{-}24h}$ values of the control (20.1 µg.h/L) and the test treatment (34.1 µg.h/L), the relative drug bioavailability would be 169.65%. The potentiality of the predicted pharmacokinetic parameters and the boosted bioavailability of VRD following the transdermal application of ETH9-INV8 system could be inferred, regardless of the population.

Compared to healthy adults, the skin physiology in geriatrics differs slightly in certain aspects like the thickness of corneocyte, the SC water content, the hair follicle density, the lipid thickness around the corneocytes and the thickness of subcutaneous tissue.[69] The plasma concentration–time curve of VRD following the transdermal application of ETH9-INV8 systemin in geriatrics showed slight differences to that predicted in adults. A higher median T_{max} and mean $AUC_{0\text{-}24h}$ values were revealed in geriatrics. Yet, a similar mean C_{max} value was predicted in both populations.

Conclusions

Ethosome-derived invasomes were successfully developed in the current work as a promising transdermal delivery system for VRD. The ex-vivo drug permeation studies, the CLSM examinations and the histopathologic assessments unraveled the enhanced skin permeation and the promising safety profile of the optimized transdermal system (ETH9-INV8). The PBPK modeling revealed the boosted bioavailability of VRD following the transdermal application of ETH9-INV8 system in adults and geriatrics. Further clinical studies are needed to explore the potential of the optimized transdermal system in patients suffering from PAH.

Disclosure

The authors report no conflicts of interest for this work.

References

1. Taichman DB, Mandel J. Epidemiology of pulmonary arterial hypertension. *Clin Chest Med*. 2013;34(4):619–637. doi:10.1016/j.ccm.2013.08.010
2. Peacock AJ, Murphy NF, McMurrey JJV, Caballero L, Stewart S. An epidemiological study of pulmonary arterial hypertension. *Eur Respir J*. 2007;30(1):104–109. doi:10.1183/09031936.00092306
3. Hoeper MM, Barberà JA, Channick RN, et al. Diagnosis, assessment, and treatment of non-pulmonary arterial hypertension pulmonary hypertension. *J Am Coll Cardiol*. 2009;54(1 Suppl):S85–96. doi:10.1016/j.jacc.2009.04.008
4. Kim D, George MP. Pulmonary hypertension. *Med Clin North Am*. 2019;103(3):413–423. doi:10.1016/j.mcna.2018.12.002
5. Archer SL, Djaballah K, Humbert M, et al. Nitric oxide deficiency in fenfluramine- and dexfenfluramine-induced pulmonary hypertension. *Am J Respir Crit Care Med*. 1998;158(4):1061–1067. doi:10.1164/ajrccm.158.4.9802113
6. Giaid A, Saleh D. Reduced expression of endothelial nitric oxide synthase in the lungs of patients with pulmonary hypertension. *N Engl J Med*. 1995;333(4):214–221. doi:10.1056/NEJM199507273330403
7. Corbin JD, Beasley A, Blount MA, Francis SH. High lung PDE5: A strong basis for treating pulmonary hypertension with PDE5 inhibitors. *Biochem Biophys Res Commun*. 2005;334(3):930–938. doi:10.1016/j.bbrc.2005.06.183
8. Karasu-Minareci E, Ozbudak IH, Ozbilim G, Sadan G. Acute effects of vardenafil on pulmonary artery responsiveness in pulmonary hypertension. *Sci World J*. 2012;2012:718279. doi:10.1100/2012/718279
9. Tantini B, Manes A, Fiumana E, et al. Antiproliferative effect of sildenafil on human pulmonary artery smooth muscle cells. *Basic Res Cardiol*. 2005;100(2):131–138. doi:10.1007/s00395-004-0504-5
10. Michelakis E, Tymchak W, Lien D, Webster L, Hashimoto K, Archer S. Oral sildenafil is an effective and specific pulmonary vasodilator in patients with pulmonary arterial hypertension: comparison with inhaled nitric oxide. *Circulation*. 2002;105(20):2398–2403. doi:10.1161/01.CIR.0000016641.12984.DC

11. Sastry BKS, Narasimhan C, Reddy NK, Raju BS. Clinical efficacy of sildenafil in primary pulmonary hypertension: A randomized, placebo-controlled, double-blind, crossover study. *J Am Coll Cardiol*. 2004;43(7):1149–1153. doi:10.1016/j.jacc.2003.10.056
12. Galiè N, Brundage BH, Ghofrani HA, et al. Tadalafil therapy for pulmonary arterial hypertension. *Circulation*. 2009;119 (22):2894–2903. doi:10.1161/CIRCULATIONAHA.108.839274
13. Rosen RC, Kostis JB. Overview of phosphodiesterase 5 inhibition in erectile dysfunction. *Am J Cardiol*. 2003;92(9A):9M–18M. doi:10.1016/S0002-9149(03)00824-5
14. Ammar HO, Tadros MI, Salama NM, Ghoneim AM. Therapeutic strategies for erectile dysfunction with emphasis on recent approaches in nanomedicine. *IEEE Trans Nanobiosci*. 2020;19 (1):11–24. doi:10.1109/TNB.2019.2941550
15. Jing ZC, Yu ZX, Shen JY, et al. Vardenafil in pulmonary arterial hypertension: A randomized, double-blind, placebo-controlled study. *Am J Respir Crit Care Med*. 2011;183(12):1723–1729. doi:10.1164/rccm.201101-0093OC
16. Tawfik MA, Tadros MI, Mohamed MI. Lipomers (lipid-polymer hybrid particles) of vardenafil hydrochloride: a promising dual platform for modifying the drug release rate and enhancing its oral bioavailability. *AAPS Pharm Sci Tech*. 2018;19(8):3650–3660. doi:10.1208/s12249-018-1191-0
17. Fahmy UA. Nanoethosomal transdermal delivery of vardenafil for treatment of erectile dysfunction: optimization, characterization, and in vivo evaluation. *Drug Des Devel Ther*. 2015;9:6129–6137. doi:10.2147/DDDT.S94615
18. Yang L, Wu L, Wu D, Shi D, Wang T, Zhu X. Mechanism of transdermal permeation promotion of lipophilic drugs by ethosomes. *Int J Nanomed*. 2017;12:3357–3364. doi:10.2147/IJN.S134708
19. Babaie S, Bakhshayesh ARD, Ha JW, Hamishehkar H, Kim KH. Invasome: A novel nanocarrier for transdermal drug delivery. *Nanomaterials*. 2020;10(2):E341. doi:10.3390/nano10020341
20. Kostewicz ES, Aarons L, Bergstrand M, et al. PBPK models for the prediction of in vivo performance of oral dosage forms. *Eur J Pharm Sci*. 2014;57:300–321. doi:10.1016/j.ejps.2013.09.008
21. Sager JE, Yu J, Ragueneau-Majlessi I, Isoherranen N. Physiologically based pharmacokinetic (pbpk) modeling and simulation approaches: a systematic review of published models, applications, and model verification. *Drug Metab Dispos*. 2015;43(11):1823–1837. doi:10.1124/dmd.115.065920
22. Zhuang X, Lu C. PBPK modeling and simulation in drug research and development. *Acta Pharm Sin B*. 2016;6(5):430–440. doi:10.1016/j.apsb.2016.04.004
23. Watt FM. Mammalian skin cell biology: at the interface between laboratory and clinic. *Science*. 2014;346(6212):937–940. doi:10.1126/science.1253734
24. Li C, Deng L, Zhang Y, Su TT, Jiang Y, Chen ZB. Silica-coated ethosome as a novel oral delivery system for enhanced oral bioavailability of curcumin. *Yao Xue Xue Bao*. 2012;47(11):1541–1547.
25. Abd-Elbary A, Makky AM, Tadros MI, Alaa-Eldin AA. Laminated sponges as challenging solid hydrophilic matrices for the buccal delivery of carvedilol microemulsion systems: development and proof of concept via mucoadhesion and pharmacokinetic assessments in healthy human volunteers. *Eur J Pharm Sci*. 2016;82:31–44. doi:10.1016/j.ejps.2015.11.006
26. Skelly JP, Shah VP, Maibach HI, et al. FDA and AAPS report of the workshop on principles and practices of *in vitro* percutaneous penetration studies: relevance to bioavailability and bioequivalence. *Pharm Res*. 1987;4(3):265–267. doi:10.1023/A:1016428716506
27. Ammar HO, Mohamed MI, Tadros MI, Fouly AA. High frequency ultrasound mediated transdermal delivery of ondansetron hydrochloride employing bilosomal gel systems: ex-vivo and in-vivo characterization studies. *J Pharm Investig*. 2020. doi:10.1007/s40005-020-00491-y.
28. Tadros MI, Fahmy RH. Controlled-release triple anti-inflammatory therapy based on novel gastroretentive sponges: characterization and magnetic resonance imaging in healthy volunteers. *Int J Pharm*. 2014;472(12):27–39. doi:10.1016/j.ijpharm.2014.06.013
29. Carlucci G, Palumbo P, Iuliani P, Palumbo G. Development of a method for the determination of vardenafil in human plasma by high performance liquid chromatography with UV detection. *Biomed Chromatogr*. 2009;23(7):759–763. doi:10.1002/bmc.1181
30. Banchroft JD, Stevens A, Turner DR. *Theory and Practice of Histological Techniques*. 4th ed. New York: Churchil Livingstone; 1996.
31. Chiu PW, Inoue H, Satodate H, et al. Validation of the quality of histological images obtained of fresh and formalin-fixed specimens of esophageal and gastric mucosa by laser-scanning confocal microscopy. *Endoscopy*. 2006;38(3):236–240. doi:10.1055/s-2005-870406
32. Stark S, Sachse R, Liedl T, et al. Vardenafil increases penile rigidity and tumescence in men with erectile dysfunction after a single oral dose. *Eur Urol*. 2001;40(2):181–188. doi:10.1159/000049770
33. Moffat AC, Osselton MD, Widdop B, eds. *Clarke's Analysis of Drugs and Poisons*. 4th ed. London: Pharmaceutical Press; 2011.
34. Ashour AE, Motiur Rahman AFM, Kassem MG. Vardenafil dihydrochloride. In: Brittain HG, editor. *Profiles of Drug Substances, Excipients and Related Methodology*. San Diego: Academic Press; 2014:515–544.
35. Mano Y, Sugiyama Y, Ito K. Use of a physiologically based pharmacokinetic model for quantitative prediction of drug-drug interactions via CYP3A4 and estimation of the intestinal availability of CYP3A4 substrates. *J Pharm Sci*. 2015;104(9):3183–3193. doi:10.1002/jps.24495
36. Tseng E, Walsky RL, Luzietti RA Jr, et al. Relative contributions of cytochrome CYP3A4 versus CYP3A5 for CYP3A-cleared drugs assessed in vitro using a CYP3A4-selective inactivator (CYP3cide). *Drug Metab Dispos*. 2014;42(7):1163–1173. doi:10.1124/dmd.114.057000
37. Abdulbaqi IM, Darwis Y, Nurzalina Khan NAK, Assi RA, Khan AA. Ethosomal nanocarriers: the impact of constituents and formulation techniques on ethosomal properties, in vivo studies, and clinical trials. *Int J Nanomedicine*. 2016;11:2279–2304. doi:10.2147/IJN.S105016
38. Vikbjerg AF, Rusig JY, Jonsson G, Mu H, Xu X. Comparative evaluation of the emulsifying properties of phosphatidylcholine after enzymatic acyl modification. *J Agric Food Chem*. 2006;54 (9):3310–3316. doi:10.1021/jf052665w
39. Abdelbary AA, Aboughaly MHH. Design and optimization of topical methotrexate loaded niosomes for enhanced management of psoriasis: application of Box-Behnken design, in-vitro evaluation and in-vivo skin deposition study. *Int J Pharm*. 2015;485(12):235–243. doi:10.1016/j.ijpharm.2015.03.020
40. Iizhar SA, Syed IA, Satar R, Ansari SA. In vitro assessment of pharmaceutical potential of ethosomes entrapped with terbinafine hydrochloride. *J Adv Res*. 2016;7(3):453–461. doi:10.1016/j.jare.2016.03.003
41. Limsuwan T, Boonme P, Amnuaikit T. Enhanced stability of phenylethyl resorcinol in elastic vesicular formulations. *Trop J Pharm Res*. 2018;13(5):472–484.
42. Garcia-Manyes S, Oncins G, Sanz F. Effect of pH and ionic strength on phospholipid nanomechanics and on deposition process onto hydrophilic surfaces measured by AFM. *Electrochim Acta*. 2006;51 (24):5029–5036. doi:10.1016/j.electacta.2006.03.062
43. Makino K, Yamada T, Kimura M, Oka T, Ohshima H, Kondo T. Temperature- and ionic strength-induced conformational changes in the lipid head group region of liposomes as suggested by zeta potential data. *Biophys Chem*. 1991;41(2):175–183. doi:10.1016/0301-4622(91)80017-L
44. Albash R, Abdelbary AA, Refai H, El-Nabarawi MA. Use of transethosomes for enhancing the transdermal delivery of olmesartan medoxomil: in vitro, ex vivo, and in vivo evaluation. *Int J Nanomed*. 2019;14:1953–1968. doi:10.2147/IJN.S196771

45. Mao YT, Hua HY, Zhang XG, et al. Ethosomes as delivery system for transdermal administration of vinpocetine. *Pharmazie*. 2013;68(5):381–382.
46. Tadros MI, Al-Mahallawi AM. Long-circulating lipoprotein-mimic nanoparticles for smart intravenous delivery of a practically-insoluble antineoplastic drug: development, preliminary safety evaluations and preclinical pharmacokinetic studies. *Int J Pharm*. 2015;493(12):439–450. doi:10.1016/j.ijpharm.2015.08.011
47. Rodriguez M, Vila-Jato JL, Torres D. Design of new multiparticulate system for potential site specific and controlled drug delivery to the colonic region. *J Control Release*. 1998;55:67–77. doi:10.1016/S0168-3659(98)00029-7
48. Rakesh R, Anoop KR. Formulation and optimization of nano-sized ethosomes for enhanced transdermal delivery of cromolyn sodium. *J Pharm Bioallied Sci*. 2012;4(4):333–340. doi:10.4103/0975-7406.103274
49. Williams AC, Barry BW. Penetration enhancers. *Adv Drug Deliv Rev*. 2004;56(5):603–618. doi:10.1016/j.addr.2003.10.025
50. Yokomizo Y. Effect of phosphatidylglycerol on the in vitro percutaneous drug penetration through the dorsal skin of guinea pigs, and analysis of the molecular mechanism, using (ATR-FTIR) spectroscopy. *Int J Pharm*. 1997;147(2):219–231. doi:10.1016/S0378-5173(96)04815-6
51. Garcia MT, Da Silva CH, De Oliveira DC, Braga EC, Thomazini JA, Bentley MV. Transdermal delivery of ketoprofen: the influence of drug-dioleylphosphatidylcholine interactions. *Pharm Res*. 2006;23(8):1776–1785. doi:10.1007/s11095-006-9040-3
52. Kriwet K, Müller-Goymann CC. Diclofenac release from phospholipid drug systems and permeation through excised human stratum corneum. *Int J Pharm*. 1995;125(2):231–241. doi:10.1016/0378-5173(95)00130-B
53. López-Pinto JM, González-Rodríguez ML, Rabasco AM. Effect of cholesterol and ethanol on dermal delivery from DPPC liposomes. *Int J Pharm*. 2005;298(1):1–12. doi:10.1016/j.ijpharm.2005.02.021
54. Scognamiglio I, De Stefano D, Campani V, et al. Nanocarriers for topical administration of resveratrol: A comparative study. *Int J Pharm*. 2013;440(2):179–187. doi:10.1016/j.ijpharm.2012.08.009
55. Dragicevic-Curic N, Scheglmann D, Albrecht V, Fahr A. Temoporfin-loaded invasomes: development, characterization and in vitro skin penetration studies. *J Control Rel*. 2008;127:59–69. doi:10.1016/j.jconrel.2007.12.013
56. Qadri GR, Ahad A, Aqil M, Imam SS, Ali A. Invasomes of isradipine for enhanced transdermal delivery against hypertension: formulation, characterization, and in vivo pharmacodynamic study. *Artif Cells, Nanomed Biotechnol*. 2017;45(1):139–145. doi:10.3109/21691401.2016.1138486
57. Chen M, Liu X, Fahr A. Skin penetration and deposition of carboxyfluorescein and temoporfin from different lipid vesicular systems: in vitro study with finite and infinite dosage application. *Int J Pharm*. 2011;408(12):223–234. doi:10.1016/j.ijpharm.2011.02.006
58. Trauer S, Richter H, Kuntsche J, et al. Influence of massage and occlusion on the ex vivo skin penetration of rigid liposomes and invasomes. *Eur J Pharm Biopharm*. 2014;86(2):301–306. doi:10.1016/j.ejpb.2013.11.004
59. El-Nabarawi MA, Shamma RN, Farouk F, Nasralla SM. Dapsone-loaded invasomes as a potential treatment of acne: preparation, characterization, and in vivo skin deposition assay. *AAPS Pharm Sci Tech*. 2018;19(5):2174–2184. doi:10.1208/s12249-018-1025-0
60. El Maghraby GMM, Williams AC, Barry BW. Interactions of surfactants (edge activators) and skin penetration enhancers with liposomes. *Int J Pharm*. 2004;276(12):143–161. doi:10.1016/j.ijpharm.2004.02.024
61. Zhao K, Singh J. In vitro percutaneous absorption enhancement of propranolol hydrochloride through porcine epidermis by terpenes/ethanol. *J Control Release*. 1999;62(3):359–366. doi:10.1016/S0168-3659(99)00171-6
62. Anjos JLVD, Neto D de S, Alonso A. Effects of 1,8-cineole on the dynamics of lipids and proteins of stratum corneum. *Int J Pharm*. 2007;345(12):81–87. doi:10.1016/j.ijpharm.2007.05.041
63. Narishetty STK, Panchagnula R. Effect of L-menthol and 1,8-cineole on phase behavior and molecular organization of SC lipids and skin permeation of zidovudine. *J Control Release*. 2005;102(1):59–70. doi:10.1016/j.jconrel.2004.09.016
64. Zhou W, He S, Yang Y, Jian D, Chen X, Ding J. Formulation, characterization and clinical evaluation of propranolol hydrochloride gel for transdermal treatment of superficial infantile hemangioma. *Drug Dev Ind Pharm*. 2015;41(7):1109–1119. doi:10.3109/03639045.2014.931968
65. Kunta JR, Goskonda VR, Brotherton HO, Khan MA, Reddy IK. Effect of menthol and related terpenes on the percutaneous absorption of propranolol across excised hairless mouse skin. *J Pharm Sci*. 1997;86(12):1369–1373.
66. Shamma RN, Aburahma MH. Follicular delivery of spironolactone via nanostructured lipid carriers for management of alopecia. *Int J Nanomed*. 2014;9:5449–5460. doi:10.2147/IJN.S73010
67. Rhee SJ, Chung H, Yi SJ, Yu KS, Chung JY. Physiologically based pharmacokinetic modelling and prediction of metformin pharmacokinetics in renal/hepatic-impaired young adults and elderly populations. *Eur J Drug Metab Pharmacokinet*. 2017;42(6):973–980. doi:10.1007/s13318-017-0418-x
68. Klotz U. Pharmacokinetics and drug metabolism in the elderly. *Drug Metab Rev*. 2009;41(2):67–76. doi:10.1080/03602530902722679
69. Cerimele D, Celleno L, Serri F. Physiological changes in ageing skin. *Br J Dermatol*. 1990;122(Suppl 35):13–20. doi:10.1111/j.1365-2133.1990.tb16120.x